Journal of Magnetic Resonance **153,** 117–123 (2001)
doi:10.1006/jmre.2001.2429, available online at http://www.idealibrary.com on IDEAL®

Proton MRI of ^{13}C Distribution by *J* and Chemical Shift Editing

C. Casieri,* C. Testa,†,‡ G. Carpinelli,† R. Canese,† F. Podo,† and F. De Luca‡,[1]

*INFM and Department of Physics, University of L'Aquila, I-67100 L'Aquila, Italy; †Laboratory of Cell Biology, Istituto Superiore di Sanità, I-00161 Rome, Italy; and ‡INFM and Department of Physics, University "La Sapienza," I-00185 Rome, Italy

Received June 1, 2001; revised July 30, 2001; published online October 5, 2001

The sensitivity of ^{13}C NMR imaging can be considerably favored by detecting the ^{1}H nuclei bound to ^{13}C nuclei via scalar *J*-interaction (X-filter). However, the *J*-editing approaches have difficulty in discriminating between compounds with similar *J*-constant as, for example, different glucose metabolites. In such cases, it is almost impossible to get *J*-edited images of a single-compound distribution, since the various molecules are distinguishable only via their chemical shift. In a recent application of *J*-editing to high-resolution spectroscopy, it has been shown that a more efficient chemical selectivity could be obtained by utilizing the larger chemical shift range of ^{13}C. This has been made by introducing frequency-selective ^{13}C pulses that allow a great capability of *indirect* chemical separation. Here a double-resonance imaging approach is proposed, based on both *J*-editing and ^{13}C chemical shift editing, which achieves a powerful chemical selectivity and is able to produce full maps of specific chemical compounds. Results are presented on a multicompartments sample containing solutions of glucose and lactic and glutamic acid in water.

Key Words: **^{13}C indirect NMR imaging; ^{13}C NMR imaging; *J*-edited NMR spectroscopy; *J*-edited NMR imaging; ^{13}C chemical shift editing; glucose metabolites imaging.**

INTRODUCTION

Direct NMR detection of ^{13}C spectra normally provides excellent molecular compound discrimination, due to a large chemical shift range that typically characterizes ^{13}C bonds (*1–3*). Conversely, from the point of view of sensitivity, the choice of directly measuring the ^{13}C spectra of molecules, especially at low concentration, can be very demanding in terms of measuring time.

A more sensitive approach to ^{13}C bonds detection is based on indirect methods implemented, for example, by selectively detecting the protons attached to each ^{13}C nucleus (*4, 5*). Besides the gain due to the higher gyromagnetic ratio of ^{1}H with respect to ^{13}C, this strategy also takes advantage of the number $n \geq 1$ of protons bound to every ^{13}C. Such an indirect approach has a very wide field of application in NMR, and appears as the most promising method for spectral detection of molecules involved in metabolic activities of living organisms, with particular attention to metabolite fluxes through glucose conversion pathways (*3*).

Many pulse sequences have been proposed to fulfill the above aims (*6, 7*). The *h*eteronuclear *s*ingle- and *m*ulti-*q*uantum *c*oherence (HSQC and HMQC) filter sequences allow good chemical resolution via the ^{13}C large chemical shift range. On the other hand, the spectral editing based on heteronuclear scalar coupling, or *J*-editing, although quite sensitive to sample motion and chemically not very selective, has good sensitivity to ^{13}C detection and owns a simple pulse sequence structure.

Chemically selective MRI methods provide unique information on the localization and extension of regions in which individual chemical species are localized. MRI can be made chemically sensitive mainly by two approaches, i.e., the so-called MR spectroscopic imaging (MRSI), in which spectra are acquired in selected volumes of the sample, and the chemical shift imaging (CSI), in which the spatial encoding is made via phase encoding only (*8–12*). Both approaches are however time-consuming and, in a complex system, provide a large amount of information that is often quite laborious to handle.

An alternative may be given by imaging a single chemical species. In such a case, the maps might result in being more "readable" and their acquisition time in being drastically reduced. For example, a biological process could be imaged by the distribution of a molecular compound representative of the biochemical mechanism involved in it. This could be achieved with an acceptable sensitivity within a shorter time, with respect to MRSI and CSI methods, which acquire the full spectral information contained in the element of spatial resolution.

Although HSQC and HMQC have also been utilized for MRSI applications on selected chemical species, with good spectral selectivity and sensitivity, their application as a routine approach may be of some difficulty, because of the complex structure of their pulse sequences (*13–15*).

The spectral editing based on *J*-coupling has, on the other hand, a simple adaptation to the imaging of a single chemical species. These methods (*16, 17*) form a class of techniques that in

[1] To whom correspondence should be addressed. E-mail: francesco.deluca@roma1.infn.it.

1090-9807/01 $35.00

general require two separate sets of scans to suppress undesired signals. Therefore, with respect to HSQC- and HMQC-MRSI, those methods are more subject to motion artifacts. For example, although the T-SEDOR (*t*win *s*pin *e*cho *d*ouble *r*esonance) *J*-editing imaging approach could, in principle, utilize a single set of data, a subtraction procedure remains necessary, because of unavoidable pulse imperfections. This situation makes T-SEDOR imaging exposed to motion artifacts and to other inaccuracies (*18, 19*). In addition, like the *J*-editing applications to spectroscopy, the imaging procedures based on *J*-selectivity cannot achieve high levels of discrimination between chemical species. On the other hand, the advantages of this approach, namely a simple pulse sequence, short measuring time, and good sensitivity, compensate in part for the drawbacks mentioned (*20, 21*).

As we have recently shown (*22*), the chemical selectivity of a *J*-based sequence such as T-SEDOR may be drastically enhanced by introducing frequency-selective ^{13}C pulses in the *J*-editing procedure. In particular, by substituting the ^{13}C hard pulses with frequency-selective soft pulses, a better *indirect* chemical resolution was obtained in spectroscopy, because of the larger ^{13}C chemical shift range with respect to that of ^{1}H nuclei.

The double-editing T-SEDOR imaging procedure proposed in this paper makes it possible to tackle the most severe difficulties in detecting one or few chemical species, in the presence of a dominant resonance coming from bulk molecules. By utilizing the ^{13}C chemical shift, a clear-cut selection was, in fact, made possible among different chemical species selected via *J*-editing. In such a way the ^{1}H signal resulted in being filtered twice, without the need of solvent (generally water) signal suppression and maintaining the benefits of proton detection, still saving the simple structure of the pulse sequence.

The main goal of this paper is to show the extent of the chemical selectivity of this imaging sequence and to prove that the inclusion of the spatial localization elements (soft pulses, slice-selective gradients, etc.) in the spectroscopic sequence (*22*) does not interfere with spectral editing. On the other hand, the sensitivity of the T-SEDOR imaging has already been demonstrated, also in an *in vivo* experiment on mouse brain, upon administration of ^{13}C-enriched glucose (*21*).

Here we report the results obtained with the T-SEDOR imaging sequence equipped with frequency-selective ^{13}C pulses, on a phantom containing water and water solutions of glucose and lactic and glutamic acid. The results showed a full spatial discrimination between all these compounds, with a gain in sensitivity given by indirect ^{13}C detection.

Although this chemical imaging approach is finalized mainly to the detection of the spatial distribution of molecules in living organisms, its possible application to other kinds of scientific areas, which also require slice selection capability, chemical selectivity, and short measurement times, should not be undervalued. Examples are studies of percolating liquids in natural or artificial lattices, measurements of the diffusion of a liquid in a liquid or of liquids in macroporous systems (*23, 24*).

METHOD AND RESULTS

The T-SEDOR sequence allows detection of ^{13}C spins by echo refocusing their *J*-coupled protons and transforming the in-phase coherence of the uncoupled protons into a nonobservable polarized state (*18, 19*). The ^{1}H T-SEDOR echo amplitude is governed by the function $\sin^2(2\pi J\tau)$, which has maxima at $\tau = (2m+1)/4J$, m being an integer: the scarce chemical selectivity of the sequence is caused just by the smooth maximum of $\sin^2(2\pi J\tau)$ vs τ. The T-SEDOR echo of coupled protons "proves" the presence of ^{13}C nuclei and produces a signal, which is about $32n$ times more sensitive than that detectable by direct ^{13}C measurement; as stated in the Introduction, n is the number of protons bound to every ^{13}C nucleus (*19*). Besides a phase-cycling routine, the averaging of transients also includes the difference between transients obtained with and without 180° pulses on ^{13}C. This reduces the indirect detection gain to $\frac{32}{\sqrt{2}}n$, but enhances the sensitivity to very low concentrations of ^{13}C, by canceling the weaker residual of an uncoupled protons signal. The 180°–^{13}C pulses make the behavior of the scalar ^{1}H–^{13}C coupling like that of a homonuclear interaction. They allow the isolation of the uncoupled protons and their conveyance into a polarized state. In the absence of the ^{13}C pulses there is neither coupled nor uncoupled ^{1}H T-SEDOR echo refocusing.

The 180°–^{13}C soft pulses of the modified T-SEDOR imaging sequence (Fig. 1) specifically selects, among the compounds picked via *J*-editing, that with a given ^{13}C spectrum (*18*). In other words, the substitution of hard pulses with soft ones makes the *J*-editing active only for ^{1}H spins coupled to the ^{13}C nuclei whose chemical shift is comprised within the spectral shape of the soft pulses. In this way, the chemical resolution is greatly increased, since the large chemical shift of ^{13}C normally allows an effective spectral selection of individual ^{1}H–^{13}C bonds.

In the sequence reported in Fig. 1, the 180°–^{1}H pulses are formed by hard pulses, while the 180°–^{13}C pulses are formed by 2-ms Gauss-shaped pulses with the central frequency chosen according to direct ^{13}C measurements. The sequence is completed by a four-step CYCLOPS phase cycling routine.

The slice selection is provided by selective ^{1}H–90° pulses and gradients, as in normal MRI (*21*). In the present case, all parameters have been set to give a slice thickness of about 4 mm. The gradients for spatial plane encoding were switched on within the second half of the sequence, with gradients acting within pulses. In this way, the spatial selectivity does not interfere with the spectral selectivity because, during the time in which the 180° pulses are on, no gradients are active.

The measurements were performed at 4.7 T (50.4 MHz for ^{13}C) on a SISCO/Varian Inova 200/183 spectrometer (Varian Associates, Inc., Palo Alto, CA) equipped with a horizontal magnet. The double-resonant probe was implemented using a circularly

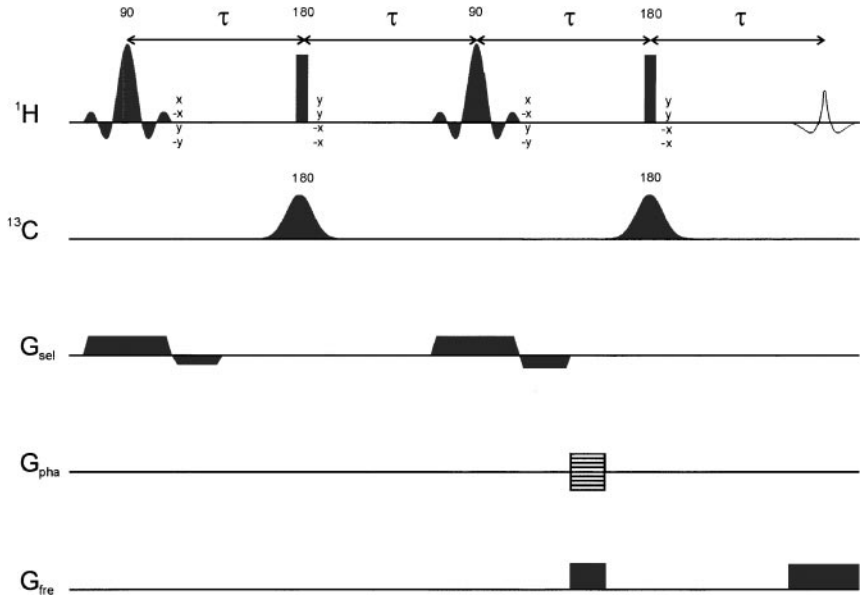

FIG. 1. Schematic representation of the T-SEDOR sequence for imaging with 180°–^{13}C soft pulses. Besides the 4-step CYCLOPS phase-cycling routine, the averaging of transients comprises also the difference between T-SEDOR echoes with and without 180°–^{13}C pulses. Actually, instead of being switched off, the 180°–^{13}C are shifted far from the ^{13}C resonance, to leave as unmodified as possible the working condition of the ^{1}H coil. The difference artifice, although halving the transients containing useful signals, allows the cancelation of the effect due to pulse imperfections by substantially increasing the sensitivity of the sequence at low ^{13}C concentration. The 180°–^{13}C soft pulses are formed by 2-ms Gauss-shaped pulses with the central frequency fixed on the molecular species to be irradiated. The imaging sequence is completed by the slice-selection gradients, which are switched on during the 90°–^{1}H pulses, and by the phase- and frequency-encoding gradients, which are switched on within the last couple of ^{1}H pulses.

polarized ^{1}H resonator (USA Instruments, Aurora, OH) with an inner homemade saddle coil for ^{13}C excitation. All images were obtained with 64 steps of a phase-encoding gradient to form a 64×64 image matrix (Fig. 1). A recycling time of 0.5 s and an interpulses delay of $\tau = 3/(4J)$ ms were used: the ^{1}H T-SEDOR echo time $4\tau = 3/J$ corresponds to the second maximum ($m = 1$) of the modulation function and depends upon the J value.

The capability of the T-SEDOR imaging sequence with ^{13}C soft pulses to effectively select different chemical species was tested on aqueous solutions of different ^{13}C-labeled glucose metabolites. To this end, we used a test object (Fig. 2a) with four cylindrical compartments, indicated by GT, LA, GC, and W, respectively containing solutions of 50% D_2O and 50% H_2O and NaCl at physiological concentrations of: (a) 200 mM [4-^{13}C]-L-glutamic acid (compartment GT; $J_{Gt} = 129$ Hz); (b) 200 mM [3-^{13}C]-L-lactic acid (compartment LA; $J_L = 129$ Hz); and (c) 200 mM [$^{13}C_6$]-D-glucose (compartment GC; $J_{1\alpha,1\beta,C2-C5} \cong 165$ Hz, $J_{C6} = 140$ Hz). The compartment W was filled with the D_2O/H_2O/NaCl solution only. All ^{13}C labels were at 99% ^{13}C isotopic substitution. A standard spin-echo image of the test object is reported in Fig. 2b. The basic parameters of this image were similar to those used for the T-SEDOR images (see below).

To assess the limitations in chemical selectivity inherent to the unmodified T-SEDOR J-editing approach, in Fig. 3 we report some images obtained by the standard T-SEDOR imaging sequence, in which 180°–^{13}C hard pulses were used. These images showed a good suppression of the uncoupled ^{1}H signal coming from the W compartment, and different signal intensities coming from the coupled protons in the GT, LA, and GC compartments. The images of Figs. 3a, 3b, and 3c were acquired taking into account the different J values of the individual compounds. In particular, that of Fig. 3a was obtained with $\tau = 5.2$ ms, corresponding to $J = 145$ Hz, which is the average of the J values of GT, GC, and LA weighted by the number of ^{13}C–^{1}H bonds of each molecule. In Fig. 3b, the τ value (4.5 ms) was optimized to match the $J_{C_2-C_5}$ constant of glucose ($\cong$165 Hz), while in Fig. 3c, $\tau = 5.8$ ms was chosen, according to the J constants of both L-glutamic and L-lactic acid ($\cong$129 Hz).

The different relative amplitudes of signals from GT, LA, and GC in Fig. 3 reflect the fact that only one carbon is substituted by ^{13}C in lactic and glutamic acid and their coupled protons are three and two, respectively, while in [$^{13}C_6$]-D-glucose seven protons are coupled to ^{13}C nuclei. The images of Fig. 3 confirm that for molecules with similar J values, the change of τ according to J is not very effective in discriminating between the different compounds. In evaluating the relative intensities of the various images, T_2 effects can be neglected, because of the very small differences between the different τ values used to match the different J coupling constants. These images can be taken as references to evaluate the improvement in chemical selectivity achievable by T-SEDOR, when the hard pulses on ^{13}C are substituted with soft ones.

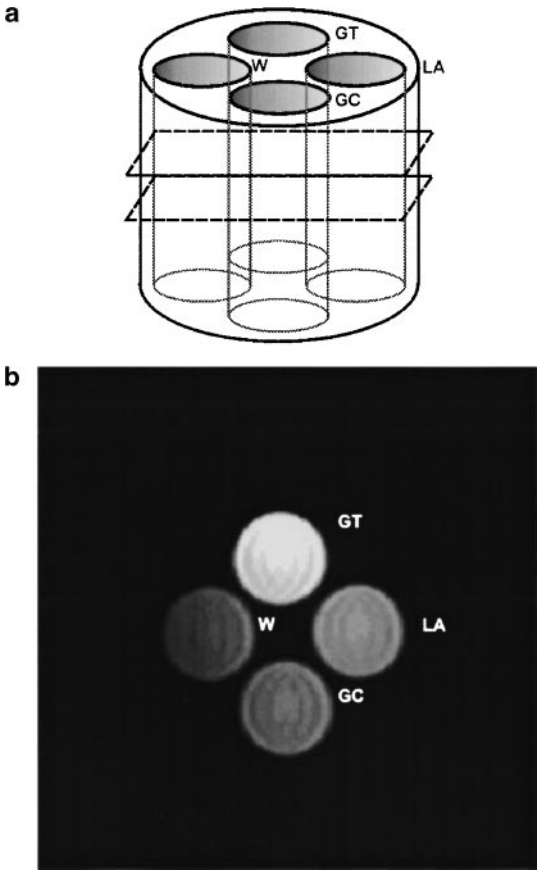

FIG. 2. (a) Schematic representation of the test object used in this work with four cylindrical compartments labeled by GT, LA, GC, and W. The slice selected by the T-SEDOR sequence is outlined by two dotted planes. The four compartments contain respectively 200 mM [4-^{13}C]-L-glutamic acid (GT), 200 mM [3-^{13}C]-L-lactic acid (LA), and 200 mM [$^{13}C_6$]-D-glucose (GC) in a physiological solution of 50% D_2O and 50% H_2O. The compartment W contains only a physiological solution of 50% D_2O and 50% H_2O. (b) A normal spin-echo image of the selected slice of both coupled and uncoupled protons is reported. Apart from the little difference in proton contents, the four compartments of the sample show different signal intensities because of the different T_2 and T_1 of the solutions. In this image, the echo time has been fixed at $2\tau' = 21$ ms ($\approx 4\tau$) and the recycling time at 0.5 s. The compartment W shows an inhomogeneity effect due probably to the coupling between the proton and the carbon coils.

The 180°–^{13}C Gaussian-shaped pulses utilized in our experiments were able to cover a spectral range of about 10 ppm out of the 80 ppm over which the ^{13}C spectrum of the whole sample is extended. The range of 10 ppm allowed the excitation of every single molecular species of the sample. In fact, the chemical shifts of the C2–C5 positions of [$^{13}C_6$]-D-glucose extend over about 7 ppm, while those of [3-^{13}C]-L-lactic acid and [4-^{13}C]-L-glutamic acid cover about 1 ppm. Furthermore, each species, as well as the C1 and C5 positions of glucose, are separated from each other by at least 10 ppm. We therefore fixed to 10 ppm the excitation range of the 180°–^{13}C pulses because this was practically the spectral resolution required to irradiate the individual components of the actual sample. Of course the range of the spectral irradiation of the 180°–^{13}C can, to some extent, also be narrowed (or expanded according to the specific requirements of the experiment).

The introduction of ^{13}C Gaussian-shaped pulses greatly enhanced the chemical selectivity of the different metabolites. In Fig. 4 three T-SEDOR images acquired with the same $\tau = 5.4$ ms, corresponding to the mean value of J (145 Hz), are reported. In Fig. 4a the frequency of ^{13}C soft pulses has been tuned on the middle of the spectrum of the C2–C5 positions of [$^{13}C_6$]-D-glucose, in Fig. 4b on that of [4-^{13}C] of L-glutamic acid, and in Fig. 4c on that of [3-^{13}C] of the L-lactic acid.

In order to allow a quantitative comparison between the results obtained from T-SEDOR sequences with and without selective 180°–^{13}C pulses, we introduced a ratio defined as

$$R_{a,b} = \frac{\Delta^{s}_{a,b} - \Delta^{ns}_{a,b}}{\Delta^{ns}_{a,b}} \cdot 100, \qquad [1]$$

where $\Delta^{s}_{a,b} = S_a - S_b$ is the difference between the average signal amplitude from samples containing the molecular species a and b, detected with 180°–^{13}C selective pulses, and $\Delta^{ns}_{a,b}$ is that detected with 180°–^{13}C hard pulses. By supposing that within the selected slice the ^{1}H equilibrium magnetization of the samples GT, GC, and LA is the same, $R_{a,b}$ of Eq. [1] represents the percentage variation of contrast between substances a and b, due to the introduction of 180°–^{13}C soft pulses, once J or τ values are fixed.

The $R_{a,b}$ values calculated from the different images, are reported in Table 1. The results obtained from the images of Fig. 4 show that, by introducing the selective spectral irradiation on ^{13}C, and fixing J to 145 Hz (the reference image with nonselective spectral irradiation being that of Fig. 3a) the contrast between the various compounds increases from about 80% between GC and LA or between GC and GT, when the 180°–^{13}C soft pulses irradiate GC, up to 2739% between LA and GT when the 180°–^{13}C soft pulses irradiate LA. The negative values on Table 1 mean that the differences in signal amplitudes between the images of Fig. 3, namely with J-selection only, are inverted with the selective irradiation. All numbers reported in Table 1

TABLE 1

$R_{GC,GT}$	$R_{GC,LA}$	$R_{LA,GT}$	180°–^{13}C	J (Hz)	Figure no.
77	81	—	GC	145	4a
−200	—	−1567	GT	145	4b
—	−309	2739	LA	145	4c
175	199	—	GC	165	5a
−218	—	−2400	GT	165	5b
—	−291	2483	LA	165	5c
36	94	—	GC	129	6a
−205	—	−4438	GT	129	6b
—	−399	7543	LA	129	6c

Note. The values of $R_{a,b}$ are calculated according to Eq. [1]. The column headed with 180°–^{13}C indicates that the 180°–^{13}C soft pulses are tuned to the specified compound. The last column reports the figure number to which all the row values refer.

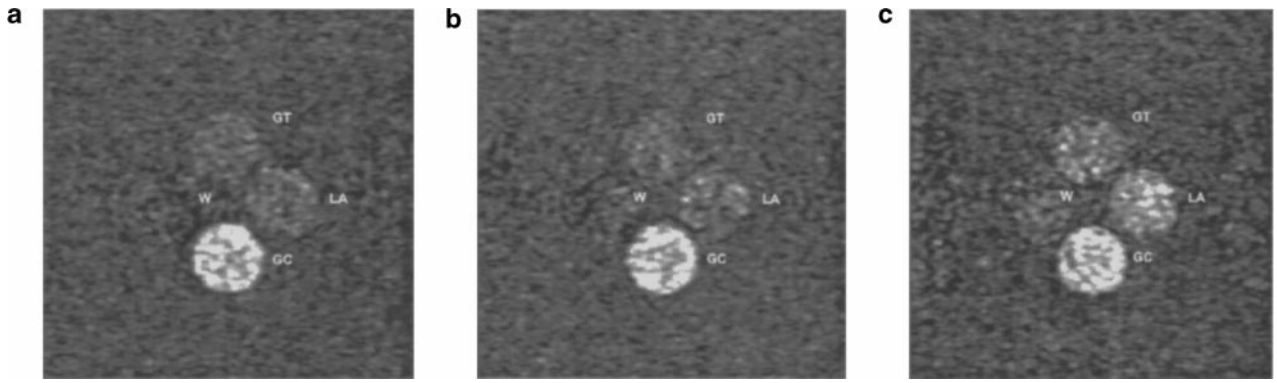

FIG. 3. ^{1}H images obtained by applying the T-SEDOR sequence with 180°–^{13}C hard pulses. The interpulse delay τ of T-SEDOR was fixed to be (a) $\tau = 3/(4\langle J\rangle) = 5.2$ ms ($J = 145$ Hz), (b) $\tau = 3/(4J_{C_2-C_5}) = 4.5$ ms ($J = 165$ Hz), and (c) $\tau = 3/(4J_{\mathrm{L}}) = 5.8$ ms ($J = 129$ Hz). These images show mainly the strong attenuation of the water signal (W compartment). The other compartments show (a) the predominance of the GC signal, the richest in coupled protons, with respect to GT and LA; (b) that the GC signal still increases due to the J value, while the signals from the compartments GT and LA are in practice the same as in (a); and (c) that the signals from the GT and LA compartments are slightly increased, while the signal from GC is still the dominant one, notwithstanding the choice of J should support the GT and LA signals.

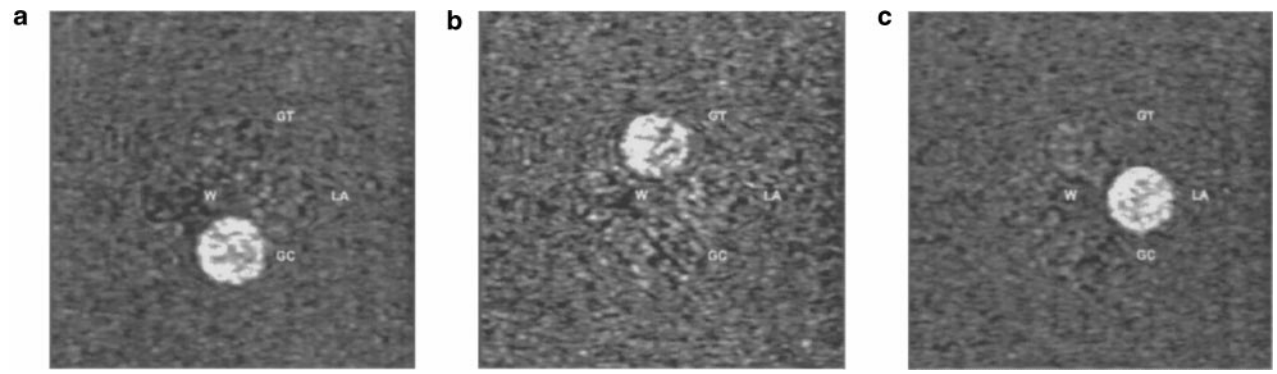

FIG. 4. ^{1}H T-SEDOR images of the same sample utilized in Fig. 3, obtained with 180°–^{13}C soft instead of hard pulses. The τ was fixed to 5.2 ms, to match $J = 145$ Hz. This parameter, as well as all others, is the same as that described in the legend to Fig. 3a. The ^{13}C pulse frequency has been tuned on (a) GC, (b) GT, and (c) LA.

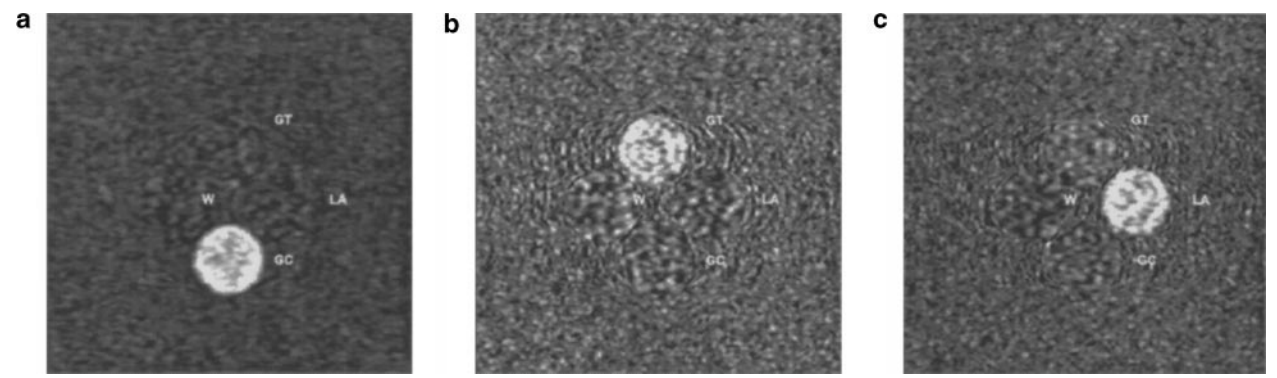

FIG. 5. ^{1}H T-SEDOR images obtained with 180°–^{13}C soft pulses. The $\tau = 4.5$ ms was fixed to match $J = 165$ Hz. This parameter, as well as all others, is the same of that described in the legend to Fig. 3b. The ^{13}C pulse frequency has been tuned on (a) GC, (b) GT, and (c) LA.

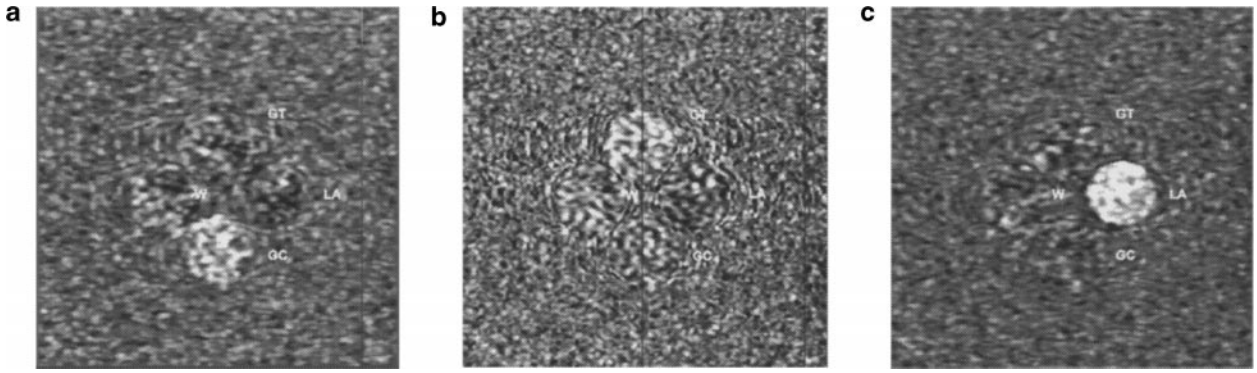

FIG. 6. ^{1}H T-SEDOR images obtained with 180°–^{13}C soft pulses. The $\tau = 5.8$ ms was fixed to match $J = 129$ Hz. This parameter, as well as all others, is the same of that described in the legend to Fig. 3c. The ^{13}C pulse frequency has been tuned on (a) GC, (b) GT, and (c) LA.

are closely dependent upon the adopted experimental setup and therefore should be intended only as an indication of the relative gain in chemical selectivity when 180°–^{13}C soft pulses are used.

In Fig. 5, τ was fixed to 4.5 ms to match $J = 165$ Hz. In the image of Fig. 5a, obtained with the 180°–^{13}C soft pulses tuned on GC, the GC contrast with respect to GT was enhanced by 175%, with respect to the value obtained in Fig. 3b (see Table 1). About the same contrast enhancement value was obtained with respect to LA. As can be seen from Table 1, the contrast enhancement between GT and LA (Figs. 5b and 5c) reached a value of about 2400%, while in Fig. 3b the signal intensity of the respective compartments was practically the same. Similar results were obtained also when τ was fixed to 5.8 ms, to match a coupling constant of $J = 129$ Hz (Fig. 6). In this case, when the 180°–^{13}C soft pulses were tuned on the GT and LA signal, the gain in contrast between these compounds reached the very substantial value of about 7500%, as reported in Table 1. The images of Fig. 6 show a signal-to-noise ratio slightly worse than those of the previous figures, giving an apparent lower contrast enhancement between GT and LA. It should be noted that the definition of $R_{a,b}$ does not take into account the noise level, this parameter being only determined from the average signal intensity in the various compartments of the sample.

CONCLUSIONS

MRI has a large availability of filters that allow the use of different chemical–physical properties of the spin system, to map the most representative NMR parameters regarding a molecular process. In this context, chemically selective MRI approaches provide particularly useful information concerning the extension and distribution of regions where the relevant chemical species are localized. The potential applications of chemically selective MRI are numerous, including *in vivo* biochemistry. It is also well known that the greatest obstacle to the development of routine chemical MRI methods is sensitivity and therefore the long measurement time needed to raise it, which especially discourages *in vivo* applications.

In this paper, we propose an approach that seems quite encouraging in the way of developing chemically selective MRI. This approach is characterized mainly by two aspects: one is related to the sensitivity and selectivity gained by detecting ^{1}H nuclei by both J and chemical shift editing; the second aspect concerns the efficacy of chemical selective MRI able to map just one single-chemical species. The first point represents the main and novel aspect of the present paper. It is known that ^{13}C spectroscopy is more effective than ^{1}H spectroscopy in discriminating between different molecular species. In this paper we suggest a way of making the chemical selectivity of T-SEDOR more effective (although a similar approach could be used in almost any X-filter sequence), that is, by utilizing soft pulses for the ^{13}C excitation. In this way, the spectral accuracy requested to get a specific ^{1}H–^{13}C map results in being notably increased, still maintaining all the advantages in sensitivity typical of the indirect ^{13}C detection. This could allow one to image many *in vivo* processes in an acceptable time, by mapping individual or few molecular compounds representative of the biochemical mechanisms involved.

The second point concerns the usefulness and advantages of single-molecule maps with respect to CSI or MRSI maps. The convenience of this approach may of course depend upon the specific aims of the experiment, but normally the distribution of a single-molecular species may be sufficient for providing relevant information, either on some biological and physiopathological processes (e.g., detection of lactate in ischemic tissues or tumors) or in material studies, such as those regarding porous systems.

On the other hand, the single-molecule map approach seems very promising from the time-consuming point of view and, therefore, from the SNR point of view, in the sense that what is saved as time may be invested to increase SNR via scans averaging. However, also supposing that none of the m molecular species involved in a process may be ignored in characterizing the space distribution of the process itself, it could prove advantageous to make m T-SEDOR images, rather than a single image made by CSI or MRSI. For example, a T-SEDOR space matrix $N \times N$ needs a time $2NT_0$ to be acquired; here T_0 is the time

needed for a single scan. For CSI, the matrix is $N \times N \times n$, where n is the number of points of the sampled spectra, so it needs a time $N^2 T_0$ to be acquired. Excluding the SNR considerations related to the proton detection of ^{13}C, a rough evaluation shows that as long as $2m < N$, acquiring the m single-chemical species maps requires a whole time that is shorter than the time needed to acquire a single CSI map.

REFERENCES

1. R. Gruetter, E. J. Novotny, S. D. Boulware, D. L. Rothman, G. F. Mason, G. I. Shulman, R. G. Shulman, and W. V. Tamborlane, Direct measurement of brain glucose concentrations in humans by ^{13}C NMR spectroscopy, *Proc. Natl. Acad. Sci. USA* **89,** 1109–1112 (1992).
2. N. R. Sibson, J. Shen, G. F. Mason, D. L. Rothman, K. L. Behar, and R. G. Shulman, Functional energy metabolism: *In vivo* ^{13}C-NMR spectroscopy evidence for coupling of cerebral glucose consumption and glutamatergic neuronal activity, *Dev. Neurosci.* **20,** 321–330 (1998).
3. J. Shen, K. F. Petersen, K. L. Behar, P. Brown, T. W. Nixon, G. F. Mason, O. A. C. Petroff, G. I. Shulman, R. G. Shulman, and D. L. Rothman, Determination of the rate of the glutamate/glutamine cycle in the human brain by *in vivo* ^{13}C-NMR, *Proc. Natl. Acad. Sci. USA* **96,** 8235–8240 (1999).
4. R. Kimmich, "NMR Tomography Diffusometry Relaxometry," Springer-Verlag, Berlin (1997).
5. R. R. Ernst, G. Bodenhausen, and A. Wokaun, "Principles of Nuclear Magnetic Resonance in One and Two Dimensions," Clarendon Press, Oxford (1987).
6. P. C. M. Van Zijl, D. Davis, S. M. Eleff, C. T. W. Moonen, R. J. Parker, and J. M. Strong, Determination of cerebral glucose transport and metabolic kinetics by dynamic MR spectroscopy, *Am. J. Physiol.* **273,** E1216–E1227 (1997).
7. S. M. Fitzpatrick, H. P. Hetherington, K. L. Behar, and R. G. Shulman, The flux from glucose to glutamate in the rat brain *in vivo* as determined by ^{1}H observed, ^{13}C-edited NMR spectroscopy, *J. Cereb. Blood Flow Metab.* **10,** 170–179 (1990).
8. P. T. Callaghan, "Principles of Nuclear Magnetic Resonance Microscopy," Clarendon Press, Oxford (1991).
9. P. Bornert, W. Dreher, A. Gossler, G. Klee, R. Peter, and W. Scheider, Chemical-shift-sensitive NMR imaging using simplification by tailored excitation, *J. Magn. Reson.* **81,** 167–172 (1989).
10. P. Bornet and W. Dreher, Chemical-shift-sensitive NMR imaging using adjusted phase encoding, *J. Magn. Reson.* **87,** 220–229 (1990).
11. A. R. Guimaraes, J. R. Baker, B. G. Jenkins, P. L. Lee, R. M. Weisskoff, B. R. Rosen, and R. G. Gonzales, Echoplanar chemical shift imaging, *Magn. Reson. Med.* **41,** 877–882 (1999).
12. L. An and Q. S. Xiang, Chemical shift imaging with spectrum modeling, *Magn. Reson. Med.* **46,** 126–130 (2001).
13. H. Watanabe, M. Umeda, Y. Ishihara, K. Okamoto, K. Oshio, T. Kanamatsu, and Y. Tsukada, Human brain glucose metabolism mapping using multislice 2D ^{1}H-^{13}C correlation HSQC spectroscopy, *Magn. Reson. Med.* **43,** 525–533 (2000).
14. P. C. M. Van Zijl, A. S. Chesnick, D. DesPres, C. T. W. Moonen, J. Ruiz-Cabello, and P. Van Gelderen, *In vivo* proton spectroscopy and spectroscopic imaging of {1-^{13}C}-glucose and its metabolic products, *Magn. Reson. Med.* **30,** 544–551 (1993).
15. Q. He, Z. M. Bhuwalla, and J. D. Glickson, Proton detection of choline and lactate in EMT6 tumors by spin-echo-enhanced selective multiple-quantum-coherence transfer, *J. Magn. Reson. B* **112,** 18–25 (1996).
16. F. Hyder, R. Renken, and D. L. Rothman, *In vivo* carbon-edited detection with proton echo-planar spectroscopic imaging (ICED PEPSI): [3,4-$^{13}CH_2$] glutamate/glutamine tomography in rat brain, *Magn. Reson. Med.* **42,** 997–1003 (1999).
17. J. W. Pan, D. T. Stein, F. Telang, J. H. Lee, J. Shen, P. Brown, G. Cline, G. F. Mason, G. I. Shulman, D. L. Rothman, and H. P. Hetherington, Spectroscopic imaging of glutamate C4 turnover in human brain, *Magn. Reson. Med.* **44,** 673–679 (2000).
18. F. De Luca, G. H. Raza, and B. Maraviglia, Low-sensitivity-nuclei localization by twin spin-echo double-resonance excitation, *J. Magn. Reson. A* **107,** 243–245 (1994).
19. F. De Luca, G. H. Raza, M. Romeo, C. Casieri, and B. Maraviglia, Twin-SEDOR spin-warp imaging of low gyromagnetic ratio nuclei, *J. Magn. Reson. B* **107,** 74–77 (1995).
20. A. Knijn, C. Casieri, G. Carpinelli, C. Testa, F. Podo, and F. De Luca, Double-resonance J-edited ^{1}H-NMR detection of [6 ^{13}C]-D 2-deoxyglucose uptake in glioma cells, *NMR Biomed.* **13,** 123–128 (2000).
21. C. Testa, C. Casieri, R. Canese, G. Carpinelli, F. Podo, and F. De Luca, *In vivo* detection of ^{13}C-enriched glucose metabolites in mouse brain by T-SEDOR imaging, *Magn. Reson. Imaging* **19,** 739–743 (2001).
22. C. Casieri, A. Knijn, F. Podo, and F. De Luca, ^{1}H NMR detection of ^{13}C-^{1}H bonds by double ^{13}C editing: Application to the discrimination of glucose metabolites, *Chem. Phys. Lett.* **338,** 137–141 (2001).
23. R. Kimmich, A. Klemm, and M. Weber, Flow, diffusion and thermal convention in percolation clusters: NMR experiments and numerical FEM/FVM simulations, *Magn. Reson. Imaging* **19,** 353–361 (2001).
24. P. Mansfiel, R. Bowtell, S. Blackband, and D. N. Guilfoyle, Magnetic resonance imaging applications of novel methods in studies of porous media, *Magn. Reson. Imaging* **126,** 1485–1489 (1992).